Ferroelectric Considerations on Co-Sputtered 30% ALSCN with Different DC+RF Ratios

Michele Pirro, Gabriel Giribaldi, Bernard Herrera Soukup, Xuanyi Zhao, Giuseppe Michetti, William Zhu, Luca Colombo, Cristian Cassella, and Matteo Rinaldi
Northeastern SMART Center, Northeastern University, Boston, USA

ABSTRACT

Aluminum-Scandium Nitride (AlScN) has recently gathered research attention due to proven ferroelectric switching along with enhanced piezoelectric coefficients [1, 2, 3]. The objective of the present work is to evaluate the impact of RF sputtering in the fabrication flow of highly-doped AlScN thin films, thus enabling new ferroelectric microelectromechanical systems (MEMS) functionalities. This paper will compare two co-sputtered 200nm AlScN films, processed with different DC to RF ratios applied to an aluminum target, highlighting the dependence of ferroelectric performance on the input signal characteristic. The work demonstrates how RF sputtering is a pivotal process-parameter in optimizing material characteristics such as coercive field and leakage current in AlScN thin films.

I. INTRODUCTION

Recently, Aluminum-Scandium Nitride (AlScN) thin film doping has been heavily investigated as a method to increase piezoelectric coefficients, as well as to reduce the material stiffness when compared with aluminum nitride (AlN) [4], [5], which would enable higher performances MEMS devices[6] without sacrificing CMOS compatibility and dielectric constants. On top of the augmented piezoelectric performances, AlScN presents ferroelectric behavior [1, 2], which could benefit established piezoelectric-based applications, such as resonators [7, 8], oscillators [9], and filters [10], as well as stimulate new MEMS-based circuit architectures. The opportunities that ferroelectric materials offer for device applications have been established in [11],[12].

Early topic explorations [13, 14, 15] highlighted two main limitations of the integration of ferroelectric AlScN: 1) the coercive field, which directly translates into hundreds of voltage for thick films; and 2) the leakage current, which could mask the effective ferroelectric switching. The present work has the objective to demonstrate how RF sputtering can be used as a leverage to ease those limitation. Triangular and trapezoidal PUND-based pulses were applied to samples deposited with different DC-to-RF power ratios, to show how high RF sputtering reduce coercive field and leakage current.

II. METHODOLOGY

Fabrication

200nm of 30% Sc-doped AlN were deposited via co-sputtering on two low-resistivity <100> oriented Si wafers with an unpatterned bottom electrode, consisting of a 20nm titanium (Ti) adhesion layer and 60nm of platinum (Pt). The tool used for the deposition is an Evatec Clusterline 200 II tool installed at Kostas Cleanroom, Northeastern University, Boston MA, USA. The two AlScN films had the same deposition conditions, except for the power applied to the aluminum target. One wafer (0-RF) was deposited by applying 1kW DC to the target, while the other (500-RF) had 500W DC and 500W RF applied. The 4" Sc target was co-sputtered at 500W DC. The deposition occurred at 350°C with a 20 SCCM N_2 flow, without pressure regulation. 400nm of Al were then sputtered and patterned for the top electrode via Cl-based Reactive Ion Etching (RIE). The whole films stacks were deposited without breaking the vacuum conditions to prevent the formation of oxide interfaces.

Material Characterization

The thickness, residual in-plane stress, and rocking curve of the fabricated films were measured using, respectively, a Woollam Ellipsometer, Flexus-Tencor, and PANalytical X'Pert Pro MPD. The measured film thicknesses for the O-RF and 500-RF samples were 200 nm and 180 nm, respectively. Such variation can be traced to the different total power applied to the Al target, which affect the deposition rate. The 0-RF sample had a residual tensile stress of 200MPa while the 500RF sample had a residual stress of 100MPa. Both wafers showed a 2θ span clean from other ASN plane directions other than [002], alluding to high-c axis orientation (Fig. 1-a). The 2θ scan showed a 0.1° shift between the two samples (Fig. 1-b), possibly indicating a few percentage points change in scandium concentration [1]. The rocking curve Full-Width-Half Maximum (FWHM) value was 2.7° for both samples, with a platinum FWHM lower than 3°.

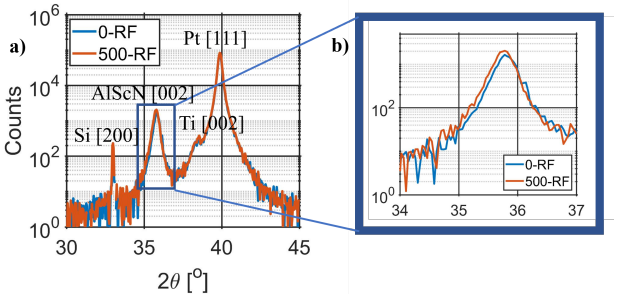

Figure 1: a) 2θ measurement with span from 30° to 45° for both sample. b) zoom-in around the AlScN-002 peaks

Electrical Characterization

An AixACCT TF2000 ferroelectric characterization tool was used to characterize the electrical and ferroelectric properties of the films. Positive-Up-Negative-Down (PUND)-based measurements were performed by applying a large voltage to the top electrode of the sample, while the bottom electrode was used as current read-out terminal by

978-1-6654-3935-0/21/$31.00 ©2021 IEEE

mean of vias etched with hot phosphoric acid. Triangular and trapezoidal PUNDs of different frequency have been used to study coercive field and leakage current.

First, triangular PUNDs were preferred to study the coercive fields, in order to avoid switching during the trapezoidal plateau. Four triangular pulses, followed by three pulses of opposite polarity were applied. If enough voltage is applied, the ferroelectric film will change its polarity direction in the 5^{th} pulse, the switching pulse. Fig. 2 compares the 2-samples output currents when switching pulses of different frequencies are applied. The ferroelectric switching is denoted by the current *hills* which make the I-E plots hysteretic. All in all, the 500-RF sample shows a smoother current transitions, higher current-values and lower fields to switch.

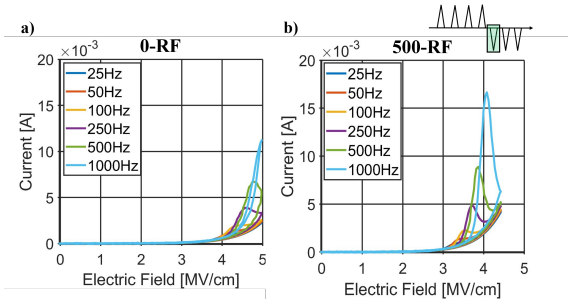

Figure 2: Output currents from 4.5MV/cm input switching voltage per different frequencies for a) 0-RF and b) 500-RF.On top of the figure, a mock-up representation of the PUND train, indicating the analyzed switching pulse.

In particular, the coercive fields variation in frequency is shown in Fig. 3. Similar trends as [16] are found. As mentioned above, the 500-RF sample requires lower voltage to switch.

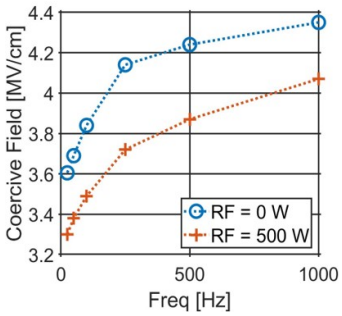

Figure 3: Coercive Field variation per different frequencies of the applied triangular signal. Red and blue lines represent the trends for the 0-RF and 500-RF samples respectively

Next, trapezoidal PUNDs were used to study the leakage current of the films, since the trapezoidal shape allows to separate capacitive and resistive currents thanks to the change in slope of the input signal. Same pulse-scheme as before, but now the 4^{th} pulse has been taken into account, the leakage pulse. In particular, from its corresponding output current, two points are highlighted: I_{tot} and I_{sta}. I_{tot} represents the output current right before the input voltage starts its DC plateau. Thus I_{tot} consists on the sum of capacitive and resistive current. On the other hand, I_{sta} is took when the input voltage goes to zero, meaning no resistive component is present. In this way, by subtracting I_{sta} from I_{tot} is possible to model the resistive behavior of the film per different applied voltage. (Fig. 4) While the 500-RF sample demonstrate a reduced resistive component in the positive leakage, no differentiation is possible when the films are negative polarized, on which >2x leakage is noticed.

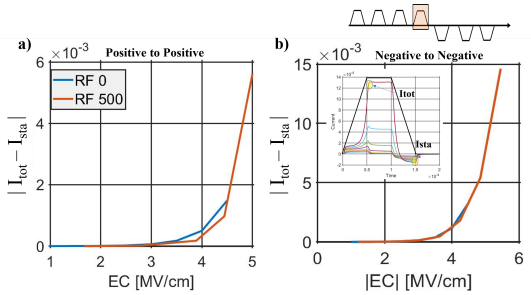

Figure 4: Variation of the resistive current per different applied field, for both sample polarity-states. a) shows positive leakage while b) the leakage when the film is polarized oppositely. The resistive component has been evaluated as the difference between I_{tot} and I_{sta} which are depicted in the inset. On top of the figure a mock up representation of the PUND train, highlighting the analyzed pulse

In order to proof the latter findings, a ferroelectric-to-leakage ratio is defined as the ratio of the maximum current to the current amplitude at the end the the trapezoidal plateau. The higher the ratio, the higher is the difference between the ferroelectric switching current and the leakage, which would simplify the polarization read-out. Fig. 5 shows the ferroelectric ratio per different applied electric field per both the switching direction, with an example of derivation on the inset. By comparing the two sample, Fig. 5a indicates how the 500-RF sample reaches an higher ration during the negative to positive switching, alluding to a smoother switching mechanism. On the other hand, no noticeable variation has been noticed in the negative-to-positive switching (Fig. 5b). On top of this, it is clear how the films have a preferred orientation: while negative to positive switching shows ratio as high as 15, the reverted polarity switching is 5x lower. All in all, these results confirm the previous finding on the leakage pulse.

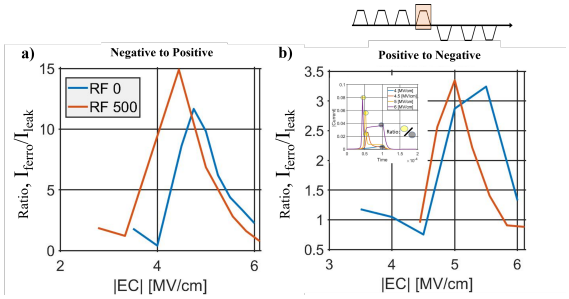

Figure 5: Electric field dependence of the ratio of the ferroelectric switching current and leakage for 0-RF and 500-RF samples for a) negative-to-positive switching and b) positive-to-negative switching. An example of ratio evaluation in the inset. On top of the figure a mock up representation of the PUND train, highlighting the analyzed pulse

III. CONCLUSION

The presented work shows the effects of RF sputtering in highly doped AlScN thin-films. Two samples with different DC to RF ratios were prepared and characterized. Different PUNDs topology have been used to properly characterize the ferroelectric properties of the films, in particular triangular PUNDs for coercive field evaluation and trapezoidal PUNDs to study the leakage. The characterization demonstrates lower coercive field and lower leakage current in the RF-500W sample. Even if more characterization is needed to confirm the effective impact of RF, this work demonstrated how RF sputtering may be the critical knob to reduce coercive field and leakage in AlScN thin films, thus enabling new MEMS applications.

ACKNOWLEDGEMENTS

This work was supported by DARPA TUFEN Program contact number HR00112090045. The authors would like to thank the staff of the George J. Kostas Nanoscale Technology and Manufacturing Research Center for assistance in device fabrication.

REFERENCES

[1] S. Yasuoka *et al.*, "Effects of deposition conditions on the ferroelectric properties of (Al1- x Sc x) N thin films," *Journal of Applied Physics*, vol. 128, no. 11, p. 114103, 2020.

[2] S. Fichtner *et al.*, "AlScN: A III-V semiconductor based ferroelectric," *Journal of Applied Physics*, vol. 125, no. 11, p. 114103, 2019.

[3] D. Wang *et al.*, "Sub-Microsecond Polarization Switching in (Al,Sc)N Ferroelectric Capacitors Grown on Complementary Metal-Oxide-Semiconductor-Compatible Aluminum Electrodes," *Physica Status Solidi rrl*, 2 2021.

[4] S. Mertin *et al.*, "Piezoelectric and structural properties of c-axis textured aluminium scandium nitride thin films up to high scandium content," *Surface and Coatings Technology*, vol. 343, pp. 2–6, 2018.

[5] M. Akiyama *et al.*, "Influence of growth temperature and scandium concentration on piezoelectric response of scandium aluminum nitride alloy thin films," *Applied Physics Letters*, vol. 95, no. 16, p. 162107, 2009.

[6] M.Moreira *et al.*, "Aluminum Scandium Nitride thin-film bulk acoustic resonators for wide band applications," *Vacuum*, vol. 86, no. 1, pp. 23–26, 2011.

[7] J. Wang, M. Park, S. Mertin, T. Pensala, F. Ayazi, and A. Ansari, "A film bulk acoustic resonator based on ferroelectric aluminum scandium nitride films," *Journal of Microelectromechanical Systems*, vol. 29, no. 5, pp. 741–747, 2020.

[8] M. Park, Z. Hao, R. Dargis, A. Clark, and A. Ansari, "Epitaxial aluminum scandium nitride super high frequency acoustic resonators," *Journal of Microelectromechanical Systems*, vol. 29, no. 4, pp. 490–498, 2020.

[9] A. Lozzi, M. Liffredo, E. T.-T. Yen, J. Segovia-Fernandez, and L. G. Villanueva, "Evidence of smaller 1/f noise in alscn-based oscillators compared to aln-based oscillators," *Journal of Microelectromechanical Systems*, vol. 29, no. 3, pp. 306–312, 2020.

[10] S. Rassay, F. Hakim, M. Ramezani, and R. Tabrizian, "Acoustically coupled wideband rf filters with bandwidth reconfigurablity using ferroelectric aluminum scandium nitride film," in *2020 IEEE 33rd International Conference on Micro Electro Mechanical Systems (MEMS)*, pp. 1254–1257, 2020.

[11] Y. Zheng, *Tunable Multiband Ferroelectric Devices for Reconfigurable RF-Frontends*. Springer, 2013.

[12] N. Setter *et al.*, "Ferroelectric thin films: Review of materials, properties, and applications," *Journal of applied physics*, vol. 100, no. 5, p. 051606, 2006.

[13] M. Pirro *et al.*, "Characterization of Dielectric and Piezoelectric Properties of Ferroelectric AlScN Thin Films," in *2021 IEEE MEMS*, IEEE.

[14] G. Giribaldi *et al.*, "Compensation of Contact Nature-Dependent Asymmetry in The Leakage Current of Ferroelectric ScxAl1−x N Thin-Film Capacitors," in *2021 IEEE MEMS*, IEEE.

[15] B. Herrera *et al.*, "AlScN Programmable Ferroelectric Micromachined Ultrasonic Transducer (FMUT)," *Transducer - Virtual Conference*, 2021.

[16] S. Fichtner, "Development of High Performance Piezoelectric AlScN for Microelectromechanical Systems: Towards a Ferroelectric Wurtzite Structure Applications," *PhD dissertation*, 2019.